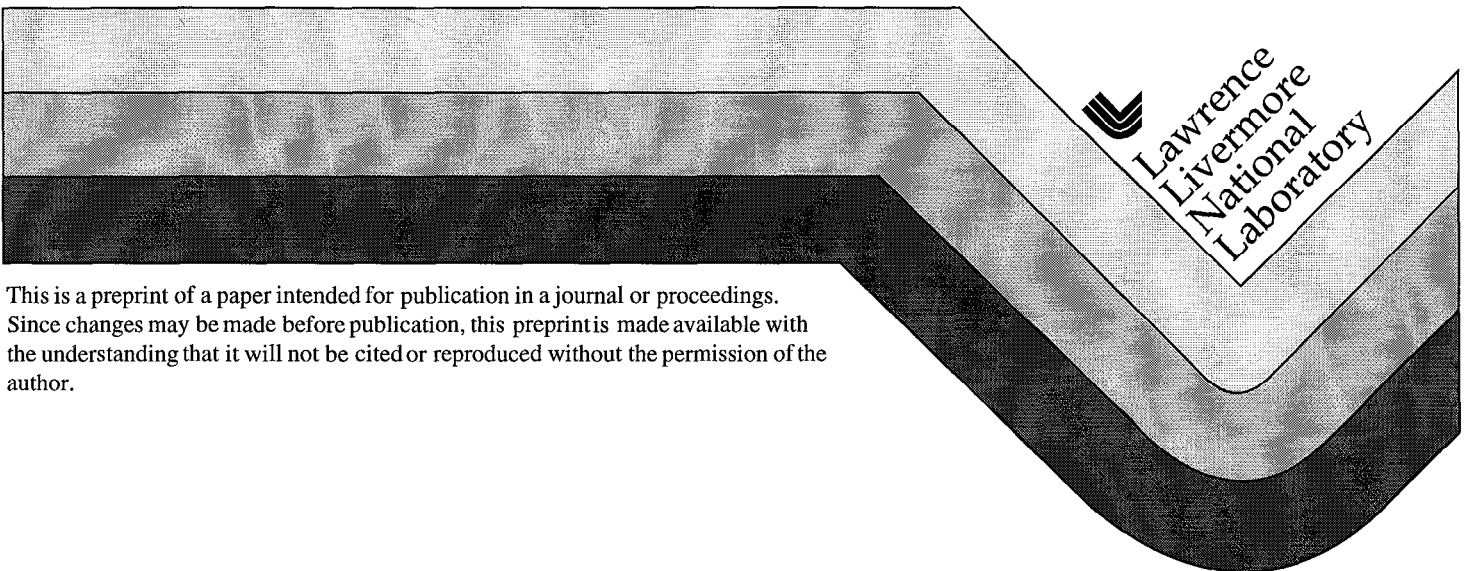


Spatial Filter Issues

J. E. Murray
D. Milam
C. D. Boley
K. G. Estabrook
F. Bonneau

This paper was prepared for submittal to the
Third Annual International Conference on
Solid State Lasers for Application (SSLA)
to Inertial Confinement Fusion (ICF)
Monterey, California
June 7-12, 1998

July 23, 1998



This is a preprint of a paper intended for publication in a journal or proceedings.
Since changes may be made before publication, this preprint is made available with
the understanding that it will not be cited or reproduced without the permission of the
author.

DISCLAIMER

This document was prepared as an account of work sponsored by an agency of the United States Government. Neither the United States Government nor the University of California nor any of their employees, makes any warranty, express or implied, or assumes any legal liability or responsibility for the accuracy, completeness, or usefulness of any information, apparatus, product, or process disclosed, or represents that its use would not infringe privately owned rights. Reference herein to any specific commercial product, process, or service by trade name, trademark, manufacturer, or otherwise, does not necessarily constitute or imply its endorsement, recommendation, or favoring by the United States Government or the University of California. The views and opinions of authors expressed herein do not necessarily state or reflect those of the United States Government or the University of California, and shall not be used for advertising or product endorsement purposes.

Spatial Filter Issues

J.E. Murray, D. Milam, C.D. Boley, K.G. Estabrook

University of California
Lawrence Livermore National Laboratory
Livermore, CA 94550 USA

F. Bonneau

Centre d'Etudes de Bruyeres-le-Chatel
Bruyeres-le-Chatel, France

ABSTRACT

Beamlet measurements show that cone pinholes outperform other types tested with regard to both closure and back reflections. A $\pm 150 \mu\text{rad}$ stainless steel cone remained open for a 15.5 kJ, 10:1 contrast shaped pulse with $\pm 7.5 \mu\text{rad}$ of SSD divergence, which more than meets the requirements for a NIF ignition pulse. Measurements also showed the maximum tolerable pressures in the NIF spatial filters to be a few milli Torr, leading to recommendations of 0.1 and 0.6 mTorr for the NIF transport and cavity spatial filters, respectively.

Keywords: pinhole closure, spatial filters, pinhole, laser-induced plasma, spatial filter pressure, back reflections

1. INTRODUCTION

We have addressed the following three spatial filter issues using the Beamlet Laser:

- Pinhole closure – How small a pinhole will stay open for the full NIF ignition pulse?
- Back reflections – How can back reflections from the pinholes be prevented?
- Spatial filter background pressure – What is the maximum allowable background pressure for the NIF cavity and transport spatial filters (CSF and TSF, respectively), and what is the effect of background pressure on pinhole closure?

2. PINHOLE CLOSURE

2.1 Pinhole types

We have tested the three types of pinholes shown schematically at the top of Fig. 1. The washer type is a simple hole in a flat

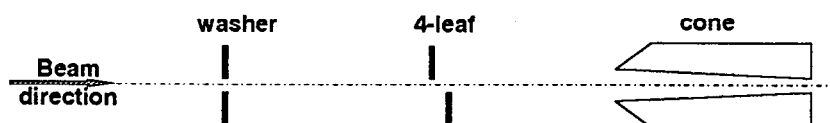
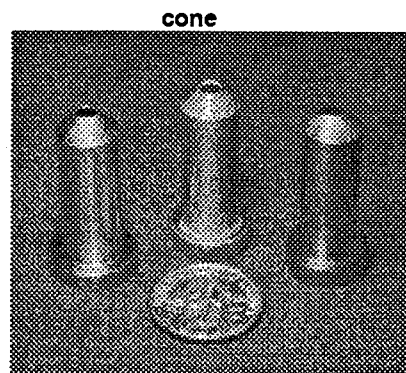
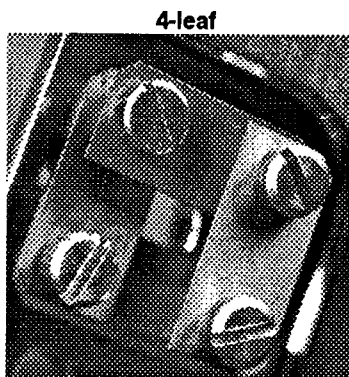


Fig. 1. The three types of pinholes tested on Beamlet

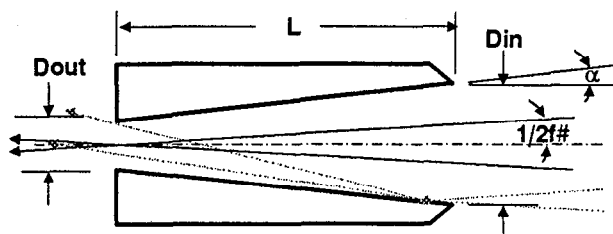


Murray 1

plate, with the plate oriented at approximately normal incidence to the beam. In the 4-leaf type the pinhole is divided into four azimuthal segments along the beam line, in order to eliminate the possibility of plasma convergence at the axis of the pinhole. The left photograph in Fig. 1 shows a rectangular (or diamond shaped) 4-leaf type. The third type is the cone pinhole¹. The right photograph in Fig. 1 shows three cone pinholes made from (left to right) stainless steel, gold, and tantalum. Since the operation of the cone type is not as obvious as the other two, and since it performed the best of the three, it will be described below in more detail.

The cone pinhole is a cylindrically symmetric section of a cone with the open end toward the beam, as shown in Fig. 2. The beam enters from the right, and the left end is positioned at the focal plane of the spatial filter lens. Given an input beam with

Fig. 2. Cross section of a cone pinhole



a specific cone half-angle, $1/2f\#$, and a desired pinhole diameter, D_{out} , the design philosophy for the cone pinhole constrains the remaining pinhole parameters:

1) Reflect or refract incoming light rather than absorb it, which leads to minimizing the cone angle α . However, the direction of the reflected/refracted light must also be changed enough to miss the clear aperture of the lens at the output of the spatial filter, to prevent it from adding to the intensity distribution of the transmitted beam. This leads to the constraint on α :

$$\alpha > \alpha_{min} = 1/2f\#$$

2) Enlarge the input diameter as much as possible to reduce plasma generation at the input end of the pinhole, which leads to maximizing the pinhole length L . In this case, the constraint results from the need to keep the reflected light from hitting the far side of the cone. The dotted lines in Fig. 2 show the worst-case rays from opposite sides of the input lens hitting the leading edge of the pinhole. These rays must pass through the output hole, which leads to the following constraint on L once α has been chosen:

$$L < L_{max} = D_{out}/(\alpha + 1/2f\#)$$

Then, given α and L ,

$$D_{in} = D_{out} + \alpha L$$

The design of all the cone pinholes tested on Beamlet was somewhat conservative, in that it did not press the limits of these constraints. The following parameters were used for the $\pm 100 \mu\text{rad}$ cone pinholes :

$$\alpha = 1.3\alpha_{min} = 25 \text{ mrad}$$

$$L = 0.7L_{max} = 29 \text{ mm}$$

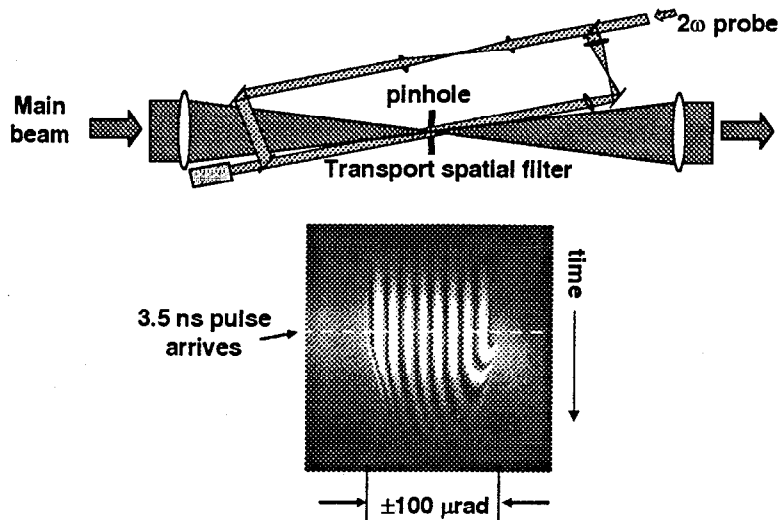
Larger pinholes used the same α and scaled L linearly with D_{out} .

2.2 Diagnostics

Three diagnostics gave the majority of the data for pinhole closure experiments on Beamlet. The first of these was a Mach-Zender interferometer to measure the phase in the pinhole during the passage of the main laser pulse. Figure 3 shows a schematic of the interferometer that was installed on the Beamlet transport spatial filter along with typical output data. The interferometer used a counter-propagating probe beam at 532 nm to protect the detectors from the main beam at 1053 nm. Its design was the same as described in another paper² presented in this session. Both a streak camera and a gated optical imager recorded the data. The streak camera showed phase changes as a function of time along a horizontal strip of the probe beam, as shown by the typical streak camera data in Fig. 3. A wedge introduced with the interferometer alignment (increasing phase from L to R) gave straight fringes with approximately uniform spacings until the pulse arrived, after which the spacings compressed on one side (L) and expanded on the other (R) as the plasma ablated away from the edges of the pinhole. The streak camera showed phase changes in the pinhole during and after the passage of the pulse.

The gated optical imager on the interferometer showed a 2-dimensional view of the interferometer fringes at a pre-set time, typically at the end of the main pulse. Its 120-ps time gate was more than adequate to completely stop fringe motion. We

Fig. 3. Schematic of interferometer installed on Beamlet, and typical streak-camera output data.

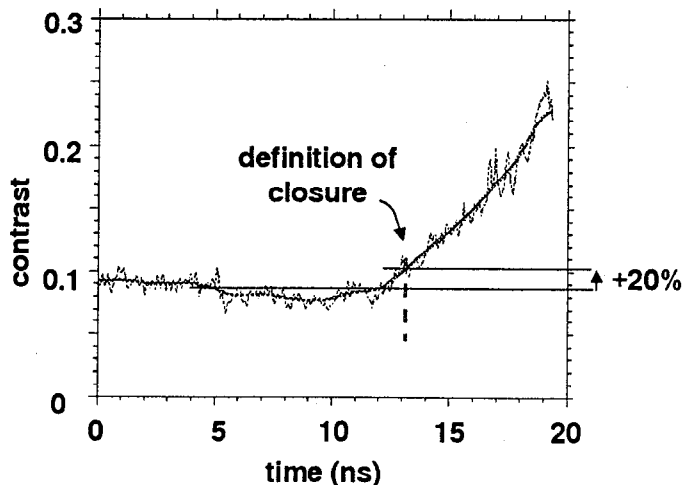


used it to watch for closure on the pinhole axis from a direction other than horizontal, which the streak camera was monitoring.

The second major pinhole closure diagnostic was a second gated optical imager looking at the near field of the beam transmitted through the pinhole. The short time gate was delayed to look within the last nanosecond of the main pulse, which was typically 20 ns long, and it therefore showed the beam distortion on the main beam at the end of the pulse. Since pinhole closure affects the trailing edge of a pulse first, this diagnostic gave the most definitive indication of closure for near threshold conditions.

The third important diagnostic was the streaked near field. A streak camera was set up to look at a central strip of the near field to show the time variation of the modulation on that strip. Since we define closure in terms of the increase in modulation on the transmitted near field, this diagnostic was used to determine when closure occurred within the pulse. Figure 4 shows an example of the processed near-field streak data for a case with obvious pinhole closure. The plot shows

Fig. 4. Typical near-field streak camera results showing definition of closure. (Contrast is defined in the main text.)



contrast, which is a measure of beam modulation, as a function of time for a 20-ns square pulse. (The heavier line is a smoothed version of the data.) Contrast is defined as the standard deviation of the modulation along the spatial direction of the streak divided by the average modulation along the same direction. Contrast starts at just under 0.1 and decreases slightly

Murray 3

for the first ~12 ns. This initial decrease is typical and is attributed to saturation in the amplifiers. At ~12 ns a sharp increase in contrast begins, which is typical of pinhole closure. We have arbitrarily defined closure time as that time when the contrast increases by 20%, as indicated in the figure. Closure times from the streak records were used with the interferometer data to determine the phase change in the pinhole at closure.

Most of the pinhole closure tests were conducted with 20-ns square pulses to simulate the leading foot of the shaped ignition pulse (see Fig. 7). To simplify comparison with shots of different energies and closure times, we found it convenient to define an $E(\text{closure})$ as the equivalent energy to close a pinhole at the end of a 20-ns square pulse. To determine $E(\text{closure})$ from a given shot, we used the following relationships: measured closure time (T) $\sim 1/(\text{closure velocity})$, closure velocity \sim intensity on pinhole edge (a result from off-line measurements on the OSL, see Ref. 2), and intensity \sim measured pulse energy (E), since we used a constant pulse shape and length. These imply that

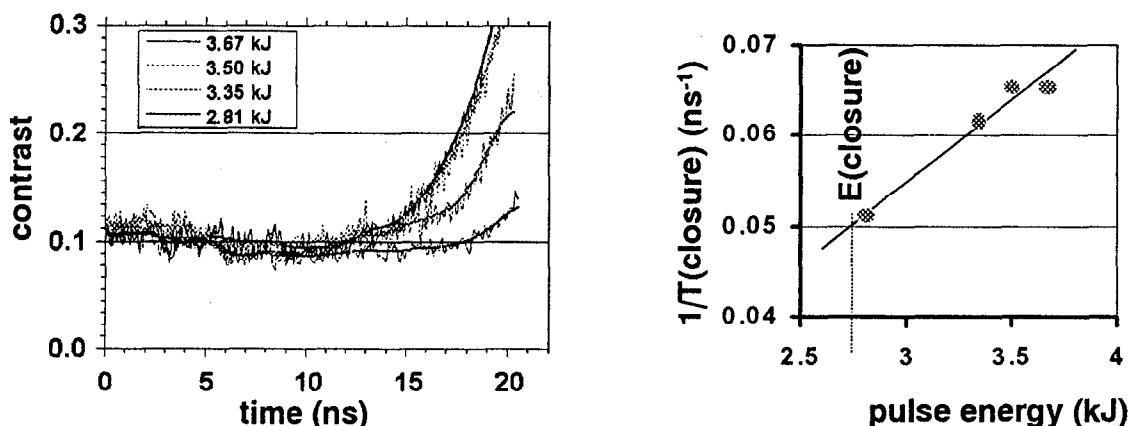
$$E_2/E_1 = T_1/T_2$$

and

$$E(\text{closure}) = E \cdot T / 20$$

Figure 5 shows an example of the use of $E(\text{closure})$ for four shots. Each used 20-ns square pulses but different pulse energies on the same $\pm 100 \mu\text{rad}$ SS cone pinhole, and, therefore, each should give the same value of $E(\text{closure})$. The left plot shows

Fig. 5 Contrast vs time from the streak records of four shots on the same pinhole, and $1/(\text{closure time})$ vs energy for those shots showing that each gives a consistent value of $E(\text{closure})$.



contrast versus time for each of the shots, as described for Fig. 4. The right plot shows $1/T$ plotted against E for each of the shots. The straight line through the data points (and the origin) shows that each is consistent with the single value of $E(\text{closure}) = 2.7 \text{ kJ}$, as required.

2.3 Experimental results

Figure 6 shows the results of all closure tests on $\pm 100 \mu\text{rad}$ cone pinholes with 20-ns square pulses. It shows $E(\text{closure})$, as defined above, plotted as a function of atomic mass for the three pinhole types and for four different materials. It shows that cone pinholes outperform washer and 4-leaf types in all cases. It also shows improved performance in general for higher atomic mass pinholes, with the exception of the gold cone, which did not perform as well as the tantalum cone. However, we believe that an inadequate finish on the interior surface of the gold cone caused its lower-than-expected performance. (More on this below.)

We also compared this 20-ns square-pulse performance of the cone pinhole to that for the shaped pulses needed for ignition experiments on NIF. The required ignition pulse at the output of the 1ω section of NIF beamlines has a contrast of 10:1. However, simple scaling laws for pinhole closure show that the hardest pinhole to keep open will not be the TSF output pinhole, but the pass-4 pinhole in the CSF. At that location, the ignition pulse, shown in Fig. 7, has a 21:1 contrast ration, which is substantially bigger than at the output due to saturation in the booster amplifiers. Measurements showed that this pulse shape closed a $\pm 100 \mu\text{rad}$ SS cone pinhole at 3x the energy of the corresponding 20-ns foot-only pulse, which is indicated by the cross-hatched region in Fig. 7. This result implies that the closure energy for ignition pulses for any one of the pinholes represented in Fig. 6 can be obtained by multiplying its $E(\text{closure})$ by three.

Fig. 6. Experimental pinhole closure results for $\pm 100 \mu\text{rad}$ cone pinholes and 20-ns square pulses

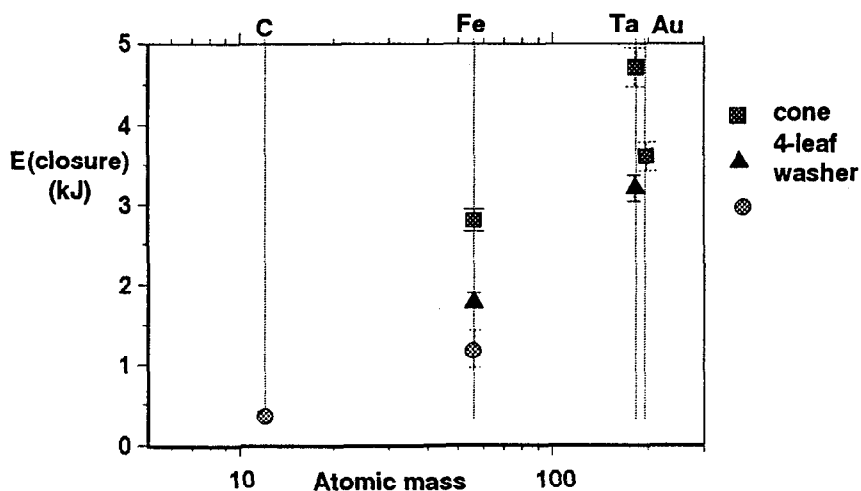
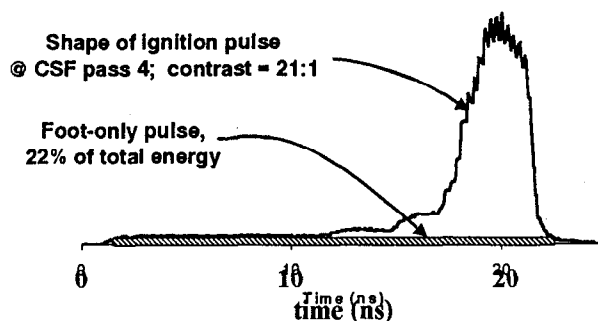


Fig. 7 Shape of a NIF ignition pulse at the pass-4 pinhole of the CSF, which will be the hardest pinhole to keep open.



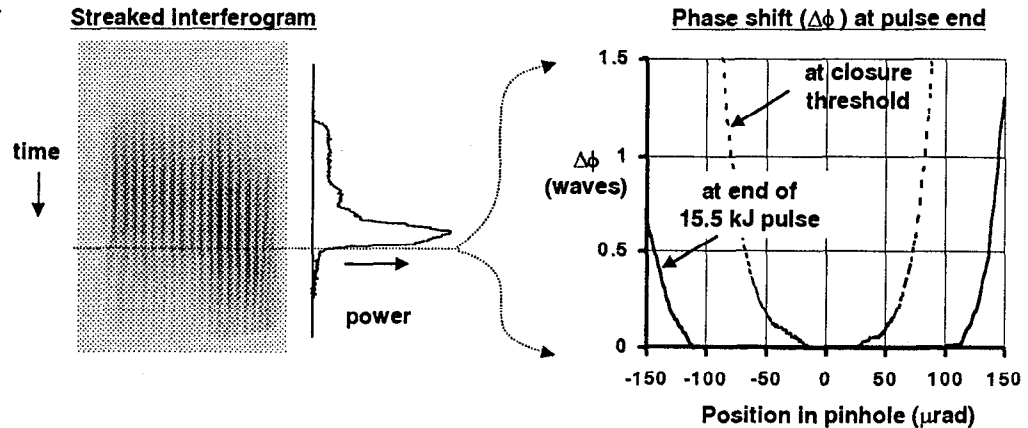
These results imply that Ta cone pinholes would be the best choice for NIF. However, Ta cone pinholes have two disadvantages compared to SS. First, they require more cleaning shots to reach optimum performance. The $E(\text{closure})$ increased with each of five consecutive shots on a $\pm 100 \mu\text{rad}$ Ta cone, whereas the same size SS cone required only one or two shots. Second, the finish of the interior surface of the cone must be very good in order for the pinholes to perform properly, and SS is easier to machine and polish than Ta. We do not know how good the finish has to be, or if it varies with pinhole material, but we do know that the Ta cone pinhole that gave the best results, $E(\text{closure}) = 4.8 \text{ kJ}$, had an $8 \mu\text{m}$ surface finish, whereas a similar Ta cone with a $30 \mu\text{m}$ finish gave $E(\text{closure}) = 2.4 \text{ kJ}$.

Propagation codes predict that the pass-4 pinhole of the CSF would have to pass 14.8 kJ to deliver 1.8 MJ of 3ω to a target. Consequently, none of the $\pm 100 \mu\text{rad}$ pinholes tested (see Fig. 6) would work for the NIF ignition pulse. The $\pm 100 \mu\text{rad}$ Ta cone comes close, based on the simple $3\times$ scaling described above, but additional margin would be needed for SSD and for a finite alignment tolerances.

On the other hand, we tested a $\pm 150 \mu\text{rad}$ SS cone pinhole, with the ignition pulse shape, and we found that this pinhole meets the NIF requirements with ease. The test propagated a 15.5 kJ , 10:1 ignition pulse with $\pm 7.5 \mu\text{rad}$ of SSD, which is the baseline SSD for NIF, and there was no sign of pinhole closure. (The 10:1 ignition pulse is harder to keep open than the required 21:1 pulse with the same total energy, because the intensity in the foot is larger by $2\times$.) Figure 8 shows the recorded phase change in the pinhole for that shot. The left figure shows the streaked interferogram with the pulse shape and the line-out at the end of the pulse. The solid curve in the plot on the right shows the phase change $\Delta\phi$ as a function of position in the pinhole for this 15.5 kJ shot. The dashed curve shows the phase change at the time of closure from a different shot. The large difference between the solid and dashed curves indicates that the $\pm 150 \mu\text{rad}$ SS cone pinhole was quite far from closure at the end of the pulse.

Murray 5

Fig. 8. Interferometric data at the pinhole for a 15.5 kJ, 10:1 contrast ignition pulse with $\pm 7.5 \mu\text{rad}$ of SSD as it passes through a $\pm 150 \mu\text{rad}$ SS cone pinhole.

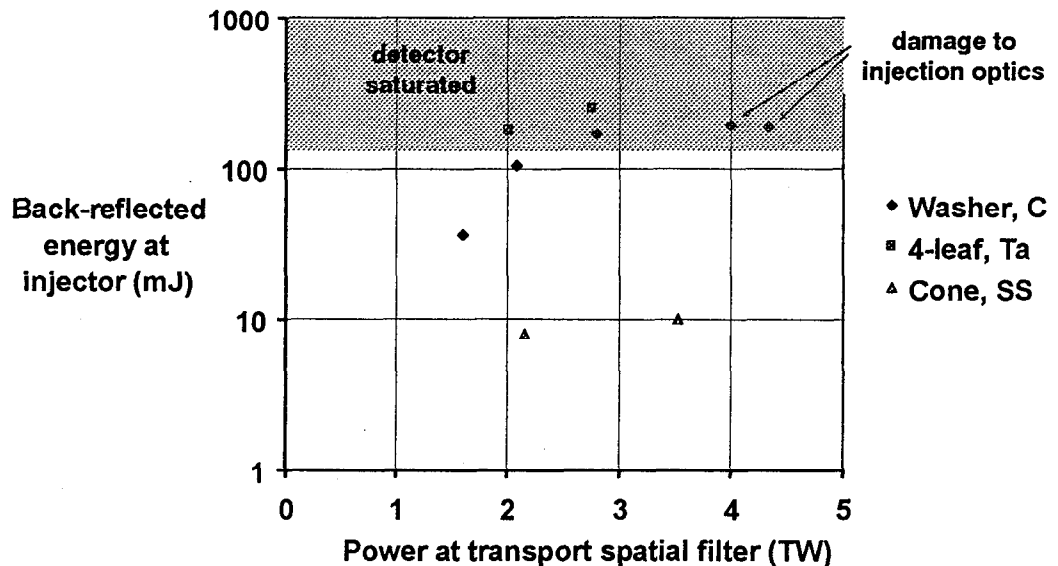


Clearly a somewhat smaller SS cone or an even smaller Ta cone would also remain open under the same conditions. However, we would have to rely on scaling to determine how small the pinhole could be made, since there will be no more full-scale pinhole testing before the first bundle of NIF is activated. Therefore, since we have this firm experimental result that meets NIF ignition pulse requirements, since Ta cone pinholes have disadvantages relative to SS, and since the NIF Project is satisfied with this large a pinhole, we suggest that the $\pm 150 \mu\text{rad}$ SS cone be made the baseline for NIF.

3. BACK REFLECTIONS FROM PINHOLES

All pinholes that we have tested back reflect for pulses greater than about 1 TW into the spatial filter. However, back reflections from cone pinholes are much less intense than those from the others. Figure 9 shows back-reflected energy

Fig. 9. Back-reflected energy at the injector versus power into the TSF, for 200-ps pulses and 3 types of $\pm 100 \mu\text{rad}$ pinholes.



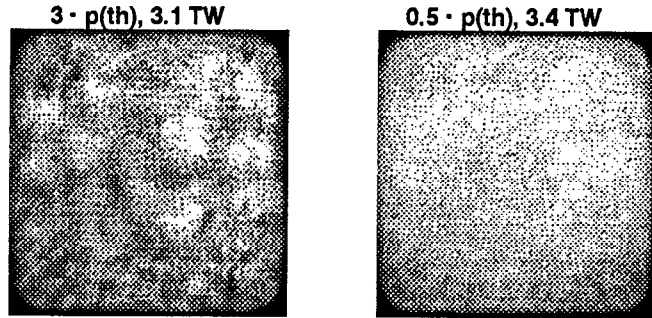
measured at the injection mirror on Beamlet versus power for the three types of $\pm 100 \mu\text{rad}$ pinholes in the TSF. Short pulses, 200 ps, were used to minimize the damage threat to Beamlet. The shading at the top of the plot shows the region in which the detector was saturated. All three of the pinhole types are represented, but the magnitude reflected from the cone pinholes is insignificant. Furthermore, it increases approximately linearly with power, whereas the back reflection for both cone and washer pinholes increases nonlinearly, indicating a stimulated scattering process at the pinhole. The two points in the upper right for C washer pinholes resulted in damage to the injection optics. Imaging of the back reflected light showed unambiguously that the back reflections originated from the surfaces of the pinhole.

Murray 6

4. MAXIMUM BACKGROUND GAS PRESSURE

Residual gas in the spatial filters at pressures above a certain threshold value, $p(\text{th})$, cause increased modulation on the near field of the pulse transmitted through the spatial filter. Figure 10 shows examples of near-field energy distributions for 200-ps pulses through a spatial filter at below and above $p(\text{th})$ and with no pinhole. Operation above $p(\text{th})$ introduces relatively

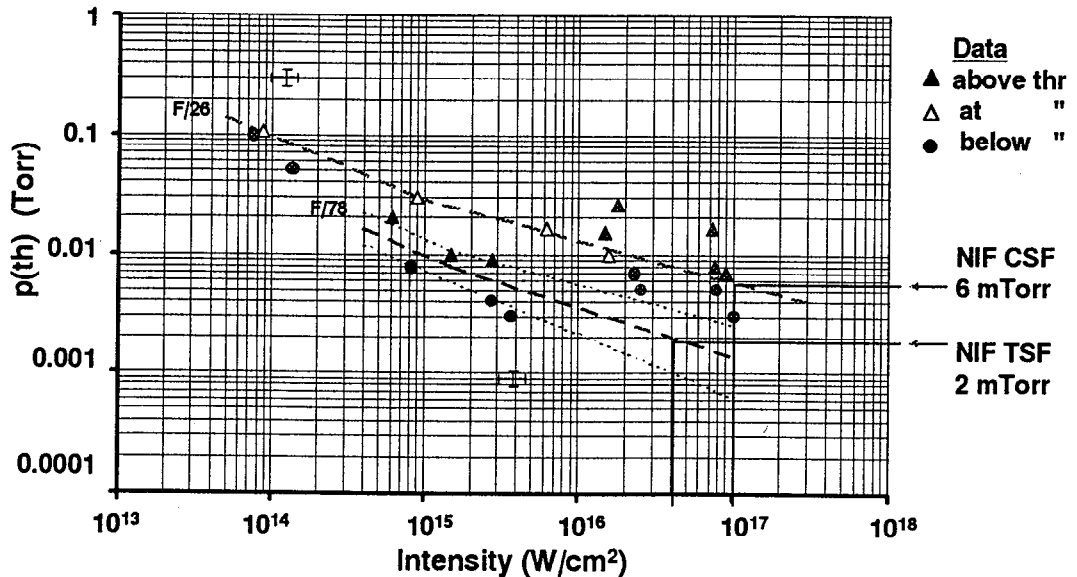
Fig. 10. Near-field energy distributions for spatial filter pressures above and below $p(\text{th})$.



long-scale modulation on the beam, similar to the modulation observed slightly above the threshold for pinhole closure.

We took a large amount of data on Beamlet to determine the values of $p(\text{th})$ for the NIF spatial filters. Figure 11 shows data plotted as pressure versus peak intensity at the focus of the spatial filter. Since we had previously demonstrated³ a strong dependence of $p(\text{th})$ on spatial filter F-number, we took data at F/26 and F/78, to simulate the NIF CSF (F/31) and TSF (F/80). For each F-number, three types of data points are distinguished in the plot, indicating above, at, and below $p(\text{th})$. Above $p(\text{th})$ is indicated by solid triangles, at $p(\text{th})$ by open triangles, and below $p(\text{th})$ by solid circles. The upper dashed curve shows $p(\text{th})$ from the F/26 data, which is well defined all the way out to the maximum intensity expected for the NIF CSF. However the F/78 data was obtained by reducing the aperture of the beam by 3x, which also reduced the maximum power output by 9x. Consequently the F/78 data ends well short of the expected intensities for the NIF TSF and had to be extrapolated. The two dotted curves show maximum and minimum credible extrapolations, and the dashed curve between shows our best-guess extrapolation.

Fig. 11. Data used to determine the threshold pressure, $p(\text{th})$, at which residual gas in spatial filters disturbs the transmitted pulse.



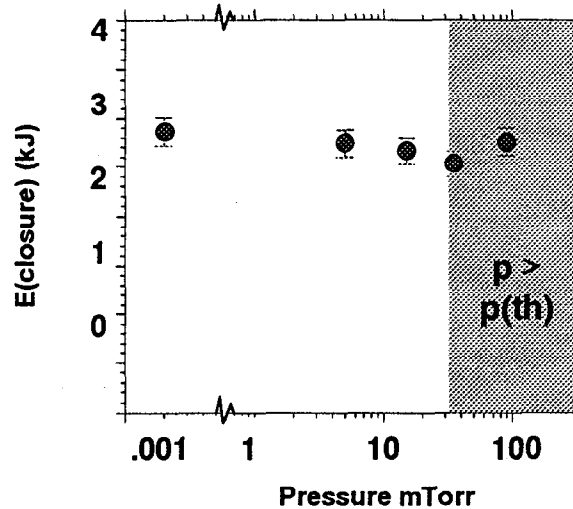
These results give $p(\text{th})$ values of 6 mTorr for the NIF CSF and 2 mTorr for the TSF. There is roughly a factor of two uncertainty in the F/78 data, because the beam quality was significantly better for the central-only part of the beam used for

Murray ?

that data, and better beam quality seems to give lower values of $p(th)$. Since, we want to allow a substantial safety factor for operational problems, we recommend that NIF operate its TSF at 0.1 mTorr. The CSF has the smaller F-number, and the NIF beam quality should be very similar to that of the full-aperture Beamlet beam, so we recommend the somewhat higher operational pressure of 0.6 mTorr.

Measurements with both a residual gas and a pinhole in the spatial filter showed no interaction between the effects of the residual gas and pinhole closure. Figure 12 shows that $E(closure)$ remains essentially constant from pressures well below to

Fig. 12. $E(closure)$ versus residual gas pressure shows no significant interaction between pinhole closure and residual gas; $\pm 100 \mu rad$ SS cone pinhole and 20-ns square pulses



3x above $p(th)$. The reason there is no interaction is that the two phenomena affect different temporal parts of the pulse. Streaked near fields showed that pressures at or slightly above $p(th)$ affect only the leading edge of the pulse, whereas near-threshold pinhole closure affects the trailing edge.

5. CONCLUSIONS

Beamlet measurements have demonstrated:

- Cone pinholes perform significantly better than washer and 4-leaf pinholes. They have higher closure energies and they back reflect less.
- A $\pm 150 \mu rad$ SS cone pinhole meets all NIF ignition pulse requirements with margin for alignment and SSD.
- The recommended operational pressures for the NIF spatial filters are 0.1 mTorr for the TSF and 0.6 mTorr for the CSF. These recommendations include a 10x safety factor.

6. ACKNOWLEDGMENTS

This work was performed under the auspices of the U.S. Department of energy by the Lawrence Livermore National Laboratory, under contract number W-7405-ENG-48.

7. REFERENCES

- ¹ P.M. Celliers, K.G. Estabrook, R.J. Wallace, J.E. Murray, L.B. Da Silva, B.J. MacGowan, B.M. Van Wouterghem, K.R. Manes, "Spatial filter pinhole for high-energy pulsed lasers", *Appl. Opt.* **37**, 2371-2378 (1998).
- ² D. Milam, J.E. Murray, E.G. Estabrook, C.D. Boley, W.D. Sell, N.D. Nielsen, R.K. Kirkwood, B.B. Afeyan and Y.A. Zakharenkov, "Pinhole Closure Measurements", these proceedings.
- ³ J.E. Murray, K.G. Estabrook, D. Milam, W.D. Sell, B.M. Van Wouterghem, M.D. Feit, A.M. Rubenchik, "Spatial Filter Issues", *Solid State Lasers for Application to Inertial Confinement Fusion*, Paris, France, 10/22 - 10/26/96, SPIE vol. 3047, pp 207-212.

Murray J